The Astrophysical Journal, 608:781–796, 2004 June 20

A DEEP *CHANDRA* X-RAY OBSERVATION OF THE RICH YOUNG CLUSTER NGC 6530. I. THE X-RAY SOURCE CATALOG AND THE CLUSTER POPULATION

F. Damiani, E. Flaccomio, G. Micela, and S. Sciortino
INAF-Osservatorio Astronomico di Palermo "G. S. Vaiana," Piazza del Parlamento 1, I-90134 Palermo, Italy; damiani@oapa.astropa.unipa.it, ettoref@oapa.astropa.unipa.it, giusi@oapa.astropa.unipa.it, sciorti@oapa.astropa.unipa.it

and

F. R. Harnden, Jr., and S. S. Murray
Smithsonian Astrophysical Observatory, 60 Garden Street, Cambridge, MA 02138
Received 2003 July 31; accepted 2004 March 2

ABSTRACT

In a deep 60 ks *Chandra* ACIS X-ray observation of the very young cluster NGC 6530, we detect 884 X-ray point sources and argue that a very large fraction of them (90%–95%) must be pre–main-sequence (PMS) cluster members, mostly of low masses. This is a significant enlargement of the known NGC 6530 stellar population with respect to previous optical studies, including Hα surveys. We identify 220 X-ray sources with cataloged stars down to $V = 17$, while most unidentified sources have fainter counterparts. Moreover, we find an infrared counterpart in the 2MASS catalog for 731 X-ray sources. The optically identified cluster X-ray sources are found in a band in the H-R diagram above the main sequence, in the locus of 0.5–1.5 Myr PMS stars, with masses down to 0.5–1.5 $M_{\odot}$. We find evidence of an age gradient across the field from northwest to south, suggesting a sequence of star formation events qualitatively similar to that found in earlier studies of the same region, but differing in the details. A group of X-ray sources showing frequent flares may be associated with the youngest stars in the cluster, suggesting that X-ray flaring activity is especially intense in the youngest PMS phases of low-mass stars.

Subject headings: open clusters and associations: individual (NGC 6530) — stars: coronae — stars: pre–main-sequence — X-rays: stars

On-line material: machine-readable table

1. INTRODUCTION

NGC 6530 is a very young cluster closely associated with the M8 nebula. This emission nebula is excited primarily by bright nearby O stars: the extremely young object Herschel 36 (O7 V), which illuminates the brightest part of M8 (the "Hourglass Nebula"), 9 Sgr (O4 V), and HD 165052 (an O6.5 V + O6.5 V binary). In addition to O stars, NGC 6530 contains about 60 B stars (Sung et al. 2000, hereafter SCB), making it ~3–4 times richer in massive stars than the Orion Nebula cluster. NGC 6530 is much farther away than the Orion Nebula: its distance has recently been estimated to be $d = 1.8$ kpc (SCB), while earlier estimates were in the range $d = 1.3$–2.0 kpc (The 1960; Walker 1957). The NGC 6530 age was estimated as ~1.5–2.0 Myr (van Altena & Jones 1972; Sagar & Joshi 1978; SCB), slightly older than the Orion Nebula cluster (Hillenbrand 1997).

The M8 emission nebula is the illuminated, nearest part of a giant molecular cloud, along the same line of sight as the visible NGC 6530 cluster, in which some of its members may be still embedded. The thick, dense molecular cloud is visible in optical images, since its nonexcited parts are dark and absorb the light of background stars. The nearly complete absence of background stars can also be verified from the H-R diagram of the cluster region (see, e.g., that shown in SCB), which shows essentially no stars fainter than the main sequence at the cluster distance for a given color.

NGC 6530 has been the subject of a number of optical studies, both to investigate its massive stars and to search for lower mass stars. Low-mass stars coeval to massive OB stars are expected to be still in their pre–main-sequence (PMS) evolutionary stages, falling above the main sequence in the cluster H-R diagram. Walker (1957) found indications of a band of less massive stars above the main sequence and tentatively identified these stars as contracting PMS stars. Later, The (1960) and Chini & Neckel (1981) found that this result was not statistically significant when compared to the local density of field stars. A proper-motion study was then made by van Altena & Jones (1972), but in excluding stars fainter than $V \sim 13.6$ they missed most of the stars hypothesized by Walker to be in the PMS stage. The existence of a PMS stellar population has therefore remained controversial until very recently. An optical study by SCB yielded only 37 (plus 9 candidate) low-mass PMS members, selected through their bright Hα emission (typical of classical T Tauri stars); since many low-mass PMS stars exist without Hα emission, this low-mass PMS sample underrepresents the true low-mass PMS cluster population. Focused mainly on the massive stars, instead, were the photometric studies by Kilambi (1977) and Sagar & Joshi (1978) and the photometric/spectroscopic study by van den Ancker et al. (1997).

NGC 6530 and M8 have also attracted attention because they provide hints of a "sequential" star formation process (Lada et al. 1976) in which the NGC 6530 cluster formed first and Herschel 36, embedded in the Hourglass Nebula about 5 pc to the west of NGC 6530, formed much more recently. Tothill et al. (2002) have studied this region at submillimeter and millimeter wavelengths and have found strings of cloud cores, which may be induced to collapse and form stars under the action of the external pressure/shock front.

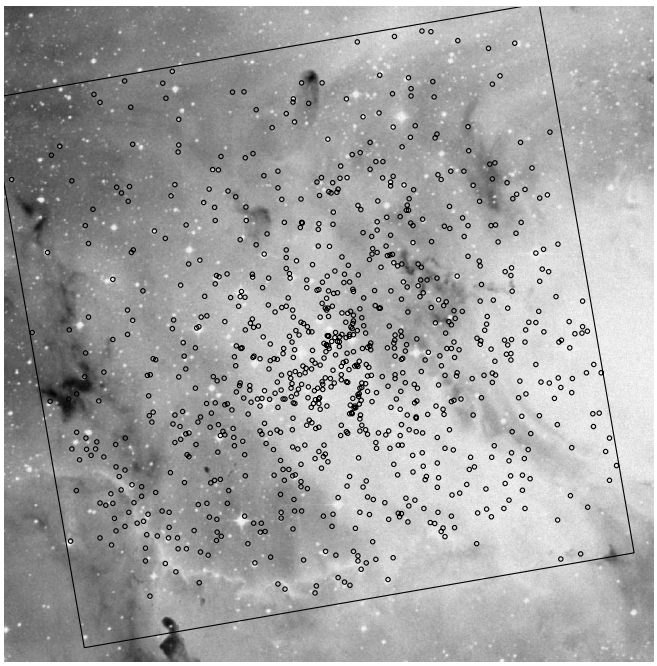

FIG. 1.—DSS red image of NGC 6530 and M8, with the ACIS-I field of view overlaid. The brightest part of the nebula, the so-called Hourglass Nebula, and its illuminating star Herschel 36 lie just outside the ACIS field. Detected X-ray sources are indicated by small circles. The ACIS-I FOV is 16.′9 on a side. North is up and east is to the left.

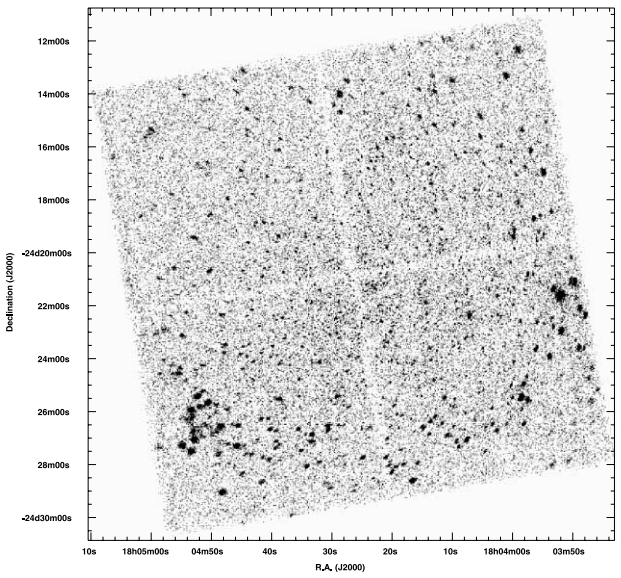

FIG. 2.—ACIS-I X-ray image of NGC 6530 in the 0.5–8.0 keV band. There are 884 X-ray point sources detected. North is up and east is to the left.

The current lack of knowledge about the bulk of the NGC 6530 stellar population has motivated us to perform an X-ray study of this cluster with the *Chandra X-Ray Observatory* (Weisskopf et al. 2002). It is well known that PMS stars have strong X-ray emission and clearly stand out in X-ray images compared to older, X-ray fainter field stars, thus enabling an accurate and efficient selection of low-mass cluster members.

M8 was recently observed in X-rays with *XMM-Newton* (Rauw et al. 2002). This observation was targeted at the Hourglass/Herschel 36 region, and only part of NGC 6530 falls in its field of view (FOV). Unlike these *Chandra* data, moreover, the *XMM-Newton* data have insufficient spatial resolution to fully resolve the dense cluster of X-ray sources. An archival *ROSAT* PSPC observation (unpublished) shows distinct X-ray sources associated with 9 Sgr and Herschel 36, but only unresolved emission ($\sim$10′ wide) coincident with the NGC 6530 center.

We present our new *Chandra* X-ray data in § 2. In § 3 we deal with the optical identification of detected X-ray sources. Section 4 contains a discussion of our results on the cluster population. A few more general conclusions on the cluster are discussed in § 5, and § 6 provides a summary of our results. The study of the ACIS X-ray spectra of NGC 6530 sources and the analysis of the properties of the X-ray emission are presented in a companion paper (F. Damiani et al. 2004, in preparation, hereafter Paper II).

2. THE X-RAY OBSERVATION AND DATA REDUCTION

NGC 6530 was observed for 60 ks with the *Chandra* ACIS-I CCD detector (Townsley et al. 2000) on 2001 June 18–19 as part of the GTO program. The ACIS-I FOV is square, 16.′9 × 16.′9, on the sky (only chips 0–3 are used). The pointing direction (R.A. = $18^{h}04^{m}24^{s}.38$, decl. = $-24^{\circ}21'05''.8$ [J2000.0]) was chosen coincident with the NGC 6530 cluster center, and because of the limited FOV we could not observe the Hourglass/Herschel 36 region, located $\sim$10′ from cluster center. Figure 1 shows a Digitized Sky Survey (DSS; second epoch) red image of NGC 6530, with the ACIS-I FOV overlaid and the positions of the X-ray–detected sources (see below).

ACIS-I images have a very narrow point-spread function (PSF; FWHM $\sim$ 0.″5 on-axis). X-ray photons are accumulated and read out every 3.2 s, so that timing analysis of not-too-intense sources can be made. The ACIS has moderate spectral resolution ($R \sim 35-50$ around 1 keV), allowing a spectral analysis to be performed.

We have inspected the ACIS background light curve to check whether high-background time intervals were present, as a consequence of eruptive solar activity. High-background episodes are capable of significantly deteriorating the data quality and must be screened out to achieve the best sensitivity for detecting sources. Fortunately, no such high-background intervals occurred during the NGC 6530 observation, and we therefore did not have to apply time filtering. As a consequence, we are able to study X-ray light curves of detected X-ray sources over an uninterrupted time span of 60 ks.

We have processed the raw X-ray event file using CIAO[1] to apply charge transfer inefficiency correction and correct for "afterglow" spurious events. We selected (standard) event grades 0, 2, 3, 4, and 6 and selected only photons in the energy range 0.3–8.0 keV. The ACIS image so obtained is shown in Figure 2 and reveals a crowded cluster of hundreds of X-ray point sources; nevertheless, it is not confused thanks to *Chandra*'s superb resolution. A zoom of the dense central region of this field is shown in Figure 3. The large number of point sources puts this cluster in a class with *Chandra* images of other massive star formation regions, such as the Orion Nebula, M17, and M16.

Source detection was performed using a 1 keV exposure map with *PWDetect*,[2] a wavelet-based source detection algorithm

[1] Ver. 2.3, http://cxc.harvard.edu/ciao.

[2] *PWDetect* is available publicly at the URL http://www.astropa.unipa.it/progetti_ricerca/PWDetect.

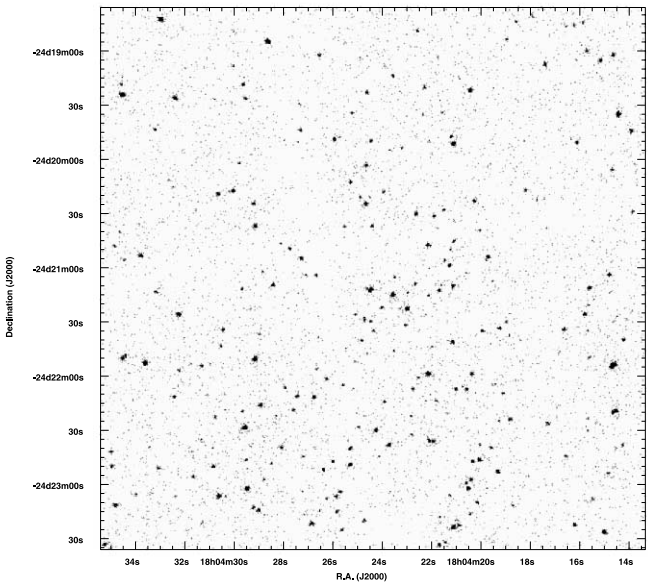

FIG. 3.—Full-resolution zoom of the central $5' \times 5'$ of the ACIS image, where spatial resolution is highest, corresponding to the NGC 6530 cluster center.

developed at the Osservatorio Astronomico di Palermo on the basis of its *ROSAT* predecessor *WDetect* (Damiani et al. 1997a, 1997b) and previously employed on *Chandra* data by Harnden et al. (2001), Flaccomio et al. (2003a, 2003b), and Damiani et al. (2003), where a brief account of its features can be found. *PWDetect* found 884 X-ray point sources in the NGC 6530 ACIS-I image, with a significance threshold chosen to ensure only one spurious detection on average. The narrow PSF and extremely low background ($\leq$0.1 counts arcsec^{-2} on-axis) of *Chandra* permit confident detection of sources with as few as 4 or 5 X-ray counts within $5'$ of field center and with 15–25 counts in the outermost field regions. Detected source count rates were measured using *PWDetect* as well. The list of detected X-ray sources in NGC 6530 is reported in Table 1. In this table we also report the probability that the X-ray source is constant according to a Kolmogorov-Smirnov test ($P_{\rm K\text{-}S}$ column), and two hardness ratios (HR1 and HR2 columns), each defined as $(H - S)/(H + S)$, where H and S are the source counts in two energy bands, here chosen as [0.75–1.5] and [0.3–0.75] keV for HR1 and [1.5–8.0] and [0.75–1.5] keV for HR2.

3. OPTICAL-INFRARED DATA AND X-RAY SOURCE IDENTIFICATION

3.1. *Available Data*

Optical data on stars in the NGC 6530 region were taken from the previous works noted in § 1, in particular from the recent work by SCB. This latter study had the deepest limiting magnitude (complete to $V = 17$, with a few stars fainter than this limit) and hence contains the largest number of stars. SCB report V magnitudes, $U-B$, $B-V$, and $V-I$ color indices, and an $R-{\rm H}\alpha$ index as a measure of Hα emission relative to the nearby continuum (analogous to the line equivalent width). Spectral types are available (from the SIMBAD database) for only 68 stars in the ACIS FOV, most having $V \leq 13$. For all other stars, the spectral type was estimated from their $B-V$ and $V-I$ colors, as in Damiani et al. (2003; their Table 7). Because of its $V = 17$ magnitude limit, only a few stars in the SCB catalog have optical colors of M stars.

As remarked in § 1, a consolidated member list is not available for stars later than about type A0, which are expected to be still contracting toward the main sequence. The proper-motion study by van Altena & Jones (1972) was complete only down to $V \sim 13.6$, corresponding to mid-A on the main sequence. Using the $R-{\rm H}\alpha$ index, SCB have selected 37 low-mass PMS members of NGC 6530, plus nine candidate members, mostly in the range $V = 14.5$–18.0. Since the SCB selection probably misses many cluster members already present in their catalog, we have cross-correlated our X-ray source catalog not with an optical list of members but with the whole SCB catalog. There are 611 SCB stars falling in our ACIS FOV.

The SCB survey does not cover the easternmost $2'.25$ of the ACIS FOV (R.A. later than $18^{\rm h}04^{\rm m}52^{\rm s}$) comprising about 13% of the FOV. There are 46 detected X-ray sources (5.2% of total) in the area not covered by SCB. The percentage of these latter sources is smaller than the uncovered area percentage because the NGC 6530 X-ray sources are strongly clustered around the center, as discussed in § 4.3.

We have also taken advantage of the availability of the 2MASS All-Sky Catalog of near-IR sources. We found 9112 2MASS sources falling in the ACIS FOV. However, following the 2MASS Explanatory Supplement (Cutri et al. 2003), we have selected only those sources unaffected by strong photometric uncertainties, discarding detections with *ph_qual* = *E*, *F*, *U*, or *X* or with *cc_flg* = *p*, *d*, or *s*. We have anyway retained sources with some confusion-related problems (*cc_flg* = *b* or *c*), a significant fraction of the total in such a crowded region. This selection results in 8792 good 2MASS sources. The number of 2MASS sources in the ACIS FOV is therefore much larger than the number of SCB stars, and moreover IR sources are less affected by extinction and can be used to probe stars embedded in the cloud or behind it.

One further advantage of using the 2MASS catalog lies in its good astrometric accuracy (80–100 mas with respect to the Tycho-2 catalog; Cutri et al. 2003). Therefore, we have matched positions of SCB stars with 2MASS sources, and after correcting for shifts of $0''.7$ in right ascension and $-0''.09$ in declination, we have found 851 SCB-2MASS identifications within $1''.3$ (of which 583 are in the ACIS FOV). Five cases of double identifications within this distance turned into single identifications by using a smaller matching distance of $0''.6$, thus obtaining a list of unique identifications.

3.2. *2MASS X-Ray Source Identification*

Since the 2MASS sample in our ACIS FOV is larger than the SCB sample and gives more accurate positions, we have first matched positions of our X-ray sources with 2MASS sources. We have used a matching distance $d < 4\ \sigma_{\rm X}$ (where $\sigma_{\rm X}$ is the *PWDetect* X-ray position error). In doing this, we found and corrected a systematic X-ray position shift of $0''.3$ in right ascension and $1''.75$ in declination (thus obtaining more accurate X-ray positions, reported in Table 1). For three X-ray sources with such a small X-ray error that $4\ \sigma_{\rm X}$ was less than $1''.5$, we relaxed the identification condition to $d < 1''.5$. This resulted in a number of multiple identifications, among which four turned into single identifications by using a reduced distance $d < 1.5\ \sigma_{\rm X}$. This leaves us with 13 double and two triple X-ray–2MASS identifications. The total number of X-ray sources with 2MASS counterpart(s) is 731, reported in Table 1. The agreement between X-ray and 2MASS positions is excellent in most cases, with offsets below $1''$.

From the total cross-identification area and the 2MASS source density we may expect 215 spurious identifications,

TABLE 1

NGC 6530 X-Ray Source Properties and Identifications

X-Ray No.	R.A. (J2000.0)	Decl. (J2000.0)	Position Error (arcsec)	Count Rate (counts ks^{-1})	$P_{K\text{-}S}$ (%)	HR1	HR2	SCB No.	Offset (arcsec)	V	$V-I$	$B-V$	2MASS	Offset (arcsec)	J	H	K
1.....	18 03 46.22	−24 25 12.2	2.05	0.891 ± 0.266	10.499	1.000	0.276	...	...	...	...	...	18034615−2425106	1.85	14.561	13.339	12.585
2.....	18 03 47.16	−24 24 22.2	1.15	1.146 ± 0.182	19.057	0.747	−0.482	203	0.81	16.094	1.660	1.288	18034720−2424212	1.08	13.022	12.142	11.608
3.....	18 03 47.21	−24 25 39.6	3.46	1.352 ± 0.346	63.661	0.644	0.426	...	...	...	...	...	18034703−2425372	3.38	13.547	11.808	10.435
3.....	18 03 47.21	−24 25 39.6	3.46	1.352 ± 0.346	63.661	0.644	0.426	...	...	...	...	...	18034745−2425372	4.08	...	...	...
4.....	18 03 47.72	−24 24 46.5	2.52	0.845 ± 0.165	75.672	1.000	−0.314	...	...	...	...	...	18034776−2424471	0.91	13.504	12.557	12.162
5.....	18 03 48.25	−24 22 23.8	0.86	4.446 ± 0.388	62.482	0.867	−0.225	209	0.40	14.835	1.383	1.073	18034826−2422233	0.51	12.339	11.743	11.497
6.....	18 03 48.48	−24 23 37.3	1.22	0.870 ± 0.159	37.274	1.000	0.641	...	...	...	...	...	18034860−2423383	2.05	13.029	11.060	10.125
7.....	18 03 49.20	−24 22 08.2	0.90	3.008 ± 0.272	0.000	0.839	0.012	222	0.74	16.636	1.636	1.252	18034920−2422084	0.32	13.623	12.883	12.613
8.....	18 03 49.28	−24 24 00.9	1.55	0.509 ± 0.174	67.449	1.000	0.222	...	...	...	...	...	...	...	...	...	...
9.....	18 03 49.33	−24 23 37.8	1.22	3.227 ± 0.285	0.000	0.917	0.093	223	0.19	16.847	1.722	1.354	18034935−2423374	0.46	13.708	12.985	12.673
10.....	18 03 50.03	−24 21 08.0	0.72	6.492 ± 0.402	0.003	0.845	−0.239	228	0.31	14.497	1.296	1.139	18035006−2421079	0.60	12.211	11.621	11.410

Notes.—Units of right ascension are hours, minutes, and seconds, and units of declination are degrees, arcminutes, and arcseconds. Table 1 is published in its entirety in the electronic edition of the *Astrophysical Journal*. A portion is shown here for guidance regarding its form and content.

more than one-quarter of the total. Since however we expect indeed a strong real correlation between our X-ray and 2MASS samples, this number is probably unrealistically large. We have therefore derived it differently. We expect the tail of the offset distribution to be more affected by spurious identifications than the distribution peak. Therefore, we counted 21 X-ray sources with identification between 3 and 4 σ, of which a significant fraction may be spurious. In particular, if we have overestimated our X-ray position error, nearly all of these 21 may be spurious identifications. Since, based on simple geometrical arguments, the number of spurious identifications in the range 3–4 σ is 43.75% of all spurious identifications within 4 σ, we would obtain a maximum total number of 48 spurious identifications in our sample. If instead our X-ray position error is correct, we expect 1.08% of all real identification to fall in the 3–4 σ range [in two dimensions, offsets are distributed as $P(r)dr = \exp(-r^2/2)r\,dr$, with r in units of σ], and thus among the 21 identifications in this range, eight will be real and 13 spurious, from which one derives a total number of 30 expected spurious identifications. To summarize, we conclude that the plausible number of spurious X-ray–2MASS identifications is between 30 and 50.

3.3. *Optical–X-Ray Source Identification*

We then performed a cross-correlation of our X-ray positions with the optical star positions of SCB, using a matching distance $d < 4\ \sigma_X$ (where σ_X is the *PWDetect* X-ray position error). In doing this, we applied a systematic shift between X-ray and SCB positions, computed from the shifts already found, of $-0\farcs4$ in right ascension and $1\farcs84$ in declination. For one X-ray source with such a small X-ray error that 4 σ_X was less than $2''$, we relaxed the identification condition to $d < 2''$. The agreement between X-ray and optical positions is again very good (see Table 1). In this case we find no ambiguous identifications, mostly because of the much smaller size of the SCB sample (limited to $V \leq 17$) compared to the 2MASS sample. In addition to the O7 star 9 Sgr, not listed by SCB but identified with the brightest X-ray source (No. 22) in the ACIS FOV, we uniquely identify 219 X-ray sources, each with an SCB optical star. Optical counterparts for the remaining 664 unidentified X-ray sources (excluding 46 sources outside the SCB surveyed region) are either fainter than $V = 17$ or are found in regions with bright nebulosity or nearby bright stars. We have also computed *PWDetect* count-rate upper limits for 391 other SCB stars that fell in the ACIS FOV but were not detected. Overall, there remain 146 X-ray sources with no optical or IR identification.

We estimate that as many as 28 of our 220 optical identifications may be spurious, with these found preferentially in the outer parts of the FOV where the ACIS PSF, positional errors, and matching distances are larger. This number is derived under the assumption that the X-ray and optical populations are uncorrelated, probably not the case for most objects in the NGC 6530 field. Analogously to the case of 2MASS identifications, it therefore should be regarded as an overestimate.

4. THE NGC 6530 CLUSTER STELLAR POPULATION

4.1. *Nonmember Contamination*

The number of X-ray sources we detect in the NGC 6530 ACIS field is so large that it leaves little doubt that most of them are indeed cluster members. Here we try to estimate more quantitatively the number of "contaminating" X-ray sources,

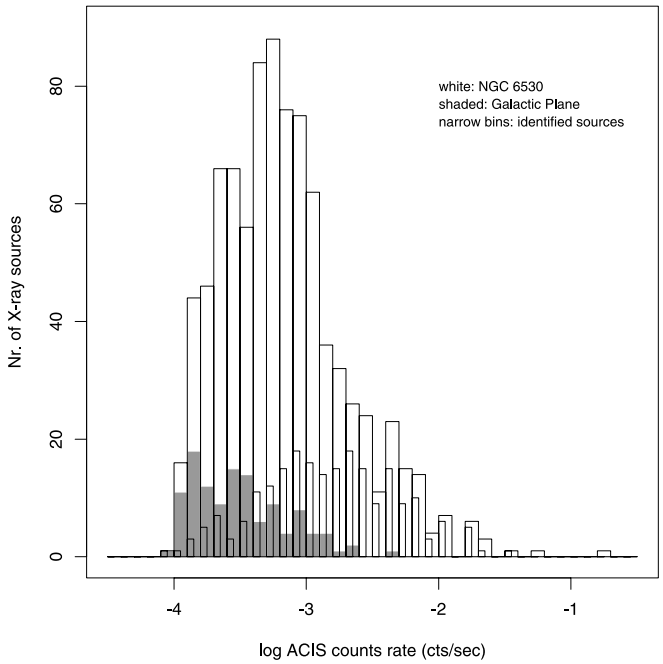

FIG. 4.—Histograms of detected source count rates in the NGC 6530 field (*white*) and in a reference Galactic plane field with the same sensitivity (*shaded*). The narrow bins indicate the count-rate distribution for optically identified sources.

which do not belong to the cluster but are either foreground or background objects. To this aim we have searched the *Chandra* data archive for other pointings toward nearby sky regions (especially at nearly the same Galactic latitude), with the same detector and with at least as long an exposure time, to be used as a "control field" for the field-object X-ray sources. There are not many archived observations meeting these requirements, and the best candidate we found is a 58 ks ACIS observation of the Galactic plane (observation ID 1523) pointed at Galactic coordinates $l = 28\fdg45$, $b = -0\fdg2$ (our NGC 6530 field is at $l = 6\fdg08$, $b = -1\fdg31$). In this field *PWDetect* detected 119 X-ray point sources (in addition to a few possible diffuse sources). This is a significantly smaller number than detected in NGC 6530. Figure 4 shows the detected count-rate distributions for NGC 6530 (*white bars*) and this Galactic plane pointing (*shaded bars*). If the number and types of field X-ray sources are the same for the Galactic plane field and NGC 6530, then most of the expected contamination occurs at the lowest X-ray fluxes, while virtually no contamination is present for count rates larger than 10^{-3} counts s^{-1}. Moreover, we have found that most of the Galactic plane X-ray sources have hard X-ray spectra (although only a handful of counts are detected for most of them), namely, harder than those of most NGC 6530 sources. Ebisawa et al. (2001) have studied this Galactic plane pointing and concluded that most of these point sources are probably extragalactic objects seen through the Galactic disk, i.e., preferentially background rather than foreground objects.

Because NGC 6530 lies in front of a dense, opaque dust cloud (see § 1), the total Galactic absorption in this direction is much larger than the simple Galactic plane value. Therefore, any background objects would be detected with still lower fluxes than those in the Galactic plane pointing. Moreover, they will be found preferentially among the hardest X-ray sources detected. Hence we estimate that the number of unrelated field

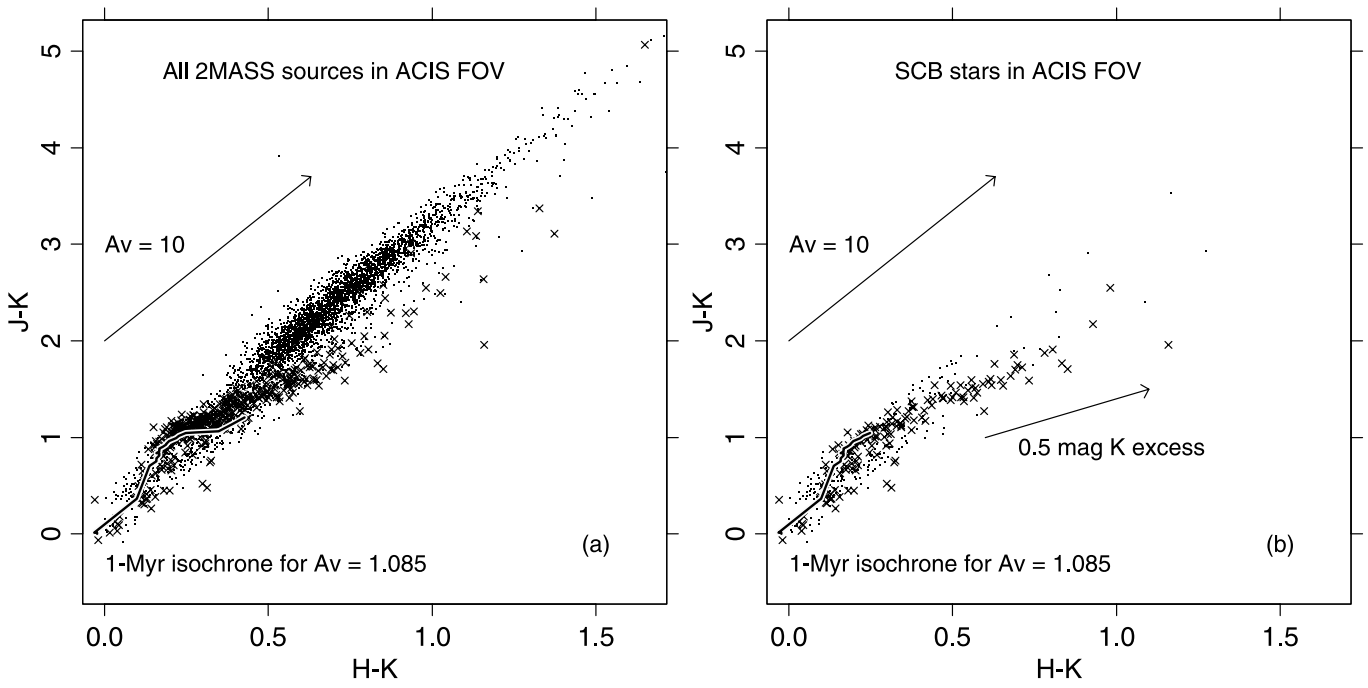

FIG. 5.—Near-IR ($H-K$, $J-K$) color-color diagram of sources in the ACIS FOV. *Crosses*: X-ray detections. *Dots*: X-ray undetected sources. The cluster-reddened 1 Myr isochrone and the reddening vector are shown. (*a*) All 2MASS sources in the FOV. (*b*) SCB stars only. In (*b*) we also show the effect of a 0.5 mag excess emission in the K band only.

objects that we detect as X-ray sources in the NGC 6530 field is definitely not larger than 120 and more probably of order ~50 objects, most of which would have very low count rates.

We plot also in Figure 4 the count-rate distribution of NGC 6530 X-ray sources that are identified with optical stars. These are more frequent at higher count rates, where the fraction of expected contaminants decreases. If we consider only optically identified X-ray sources, the number of expected detected nonmembers (computed as $\sum_i N_i^{\rm GalPl} N_i^{\rm ident}/N_i^{\rm tot}$, where the sum runs over count-rate bins and $N^{\rm GalPl}$, $N^{\rm tot}$, and $N^{\rm ident}$ are the numbers of detections in the Galactic plane field, the total number of detections in NGC 6530, and the number of optically identified sources in NGC 6530, respectively) drops to 17 at most, and is probably much lower. We conclude therefore that at least 90% of the X-ray sources detected in NGC 6530 are very probable cluster members, and this percentage rises to 95%, considering only sources with optical counterparts in the SCB catalog.

4.2. *Background/Embedded Stars from 2MASS Data*

Using 2MASS IR data, we have tried to obtain more clues about the nature of objects falling in the ACIS FOV, and in particular of detected X-ray sources. Figure 5*a* shows an ($H-K$, $J-K$) color-color diagram for all 2MASS sources in the ACIS FOV with a valid detection in the J, H, and K bands (*small dots*), with crosses indicating X-ray detected sources. Also shown are the reddened 1 Myr isochrone between 0.16 and 7 $M_\odot$ (see § 4.5; in this diagram, it is very similar to the ZAMS) and the reddening vector (from Rieke & Lebofsky 1985). Figure 5*b* is an analogous diagram including only SCB stars in the FOV. Figure 5*a* shows that most 2MASS sources in the field are found distributed in a strip nearly parallel to the extinction vector up to $H-K \sim 1.7$. The largest $H-K$ for stars with $A_V \sim 1$ is about 0.4, and therefore the much larger values of $H-K$ found are indicative of high reddening ($A_V \sim 5$–15 for most sources and ranging up to $A_V \sim 30$). Only about 60 of these high-reddening 2MASS sources are X-ray detected, very compatible with the expected number of background X-ray sources (§ 4.1). Most X-ray detections are instead found along the 1 Myr cluster isochrone, indicating low-reddening, normal photospheric emission. Some X-ray sources show redder IR colors, but not along the reddening vector, suggesting possible IR excesses from circumstellar dust.

Figure 5*b* contains only SCB stars (with $V < 17$), and we can see that while the pattern of X-ray–detected sources has not basically changed, the strip of heavily absorbed sources has almost disappeared. In particular, there are no more X-ray–detected, high-extinction sources. Therefore, while among IR-identified X-ray sources we find a few tens of sources with $A_V \sim 5$–15, virtually no such high extinction is found among optically identified X-ray sources (within the SCB limit). In either case, most X-ray sources are compatible with stars with normal IR colors and reddening in a small range ($A_V \sim$ 1–2), apart from stars with probable IR excesses. Therefore, embedded/background stars are present in a small number among X-ray sources with an IR counterpart but are effectively absent among X-ray sources with an optical (SCB) counterpart.

Since X-ray sources identified with SCB stars will be found to have a mass larger than 0.5 $M_\odot$ (see § 4.5 and Fig. 11), we have plotted in Figure 5*b* the 1 Myr isochrone only down to 0.5 $M_\odot$, and one sees that many X-ray sources now fall *redward* of it (larger $H-K$), as if they had normal colors but a lower mass, discrepant with optical photometry. If the evolutionary tracks are correct, the solution of this discrepancy might be that IR excesses are more frequent among these stars than is evident at first sight: the displacement of data points (*crosses*) in Figure 5*b* with respect to normal colors can in fact be accounted for simply by excess emission in the K band, as shown in the figure. Although a very crude approximation of a real excess-emission spectrum, this "excess vector" has the

right slope to fit the data, while the usual reddening vector does not. Moreover, postulating large reddenings ($A_V \sim 5$) for these (many) stars would imply that they are not late-type stars (see § 4.4) but a cluster of X-ray–emitting A stars, an extremely unlikely circumstance. Therefore, IR excess emission may be more widespread in our NGC 6530 stars than suggested by their apparently normal (i.e., photospheric) IR colors. Beyond these simple conclusions, the richness of 2MASS data deserves a much deeper study, which we defer to a future paper. Because of the very likely presence of IR excesses in these stars (possibly not only in the *K* band), we do not attempt to derive star properties (masses, ages) from an IR color-magnitude diagram, despite the number statistics of IR-identified X-ray sources being much larger than those of optically identified ones.

4.3. *Cluster Census and Morphology*

We are confident that about 800 of the X-ray sources that we detect in our ACIS field are confirmed cluster members (see § 4.1). This number is 8–10 times the number of confirmed NGC 6530 members known from previous optical studies. Since all higher mass stars in the cluster are already known, these new X-ray objects must correspond to lower mass stellar members (or to embedded, heavily absorbed massive stars missed by previous studies). Given that only 46 low-mass members (and candidates) were found by SCB, the increase brought about by our X-ray data in the known cluster population in this mass range is by about a factor of 15. Rauw et al. (2002), on the basis of their *XMM-Newton* X-ray data with its smaller source sample, inferred an enlargement of only a factor of 2 with respect to optical studies.

With this enlarged membership, we have attempted to study the morphology of NGC 6530. The small uncertainty related to field objects will have a minimal impact on this study, since these have a uniform spatial distribution. As seen in Figures 1 and 2, clustering of X-ray sources is highest near field center. The northeast part of the FOV has a significantly lower density, while toward the southeast a subclustering of X-ray sources can be seen. Directly counting the source density in these figures may be misleading, however, because the point-source sensitivity decreases toward the outer parts of the FOV; some central enhancement can be expected even for a uniform source density in the sky. Therefore, we plot in Figure 6 the density of sources with ACIS count rate $\geq 3 \times 10^{-4}$ counts s^{-1}, detectable across the whole FOV. This plot confirms that a strong central clustering is present, with the source density reaching a maximum at R.A. = $18^{\rm h}04^{\rm m}25^{\rm s}$, decl. = $-24^\circ 22' 00''$, which we therefore take as the NGC 6530 cluster center, and falling by a factor of 2 within a radius of $\sim 3'$ (1.5 pc) from the center. The peak density of sources with rate $\geq 3 \times 10^{-4}$ counts s^{-1} is about 46.5 stars pc^{-2} (the total peak density is 61.5 stars pc^{-2}). Figure 6 shows also that the NGC 6530 source density does not fall equally steeply in all directions. In the figure, the arrow in the top gray scale indicates the average source density (above the same full-FOV flux threshold) for the Galactic plane field. In the northeast NGC 6530 quadrant, the source density is the lowest and approaches that of the Galactic plane, while in the other three quadrants (especially in the two southern ones) it remains higher than that, until the farthest off-axis positions.

We conclude therefore that our observation has probably reached the cluster outer border in the northeast, while the cluster may extend beyond our FOV in other directions. Since the cluster center, identified as the position with the highest stellar density, appears to be near the center of our FOV, the cluster shape is asymmetrical with respect to its center. Indeed, we know that at least one young star associated with NGC 6530, namely Herschel 36, lies outside our ACIS FOV, a couple of arcminutes beyond its western edge.

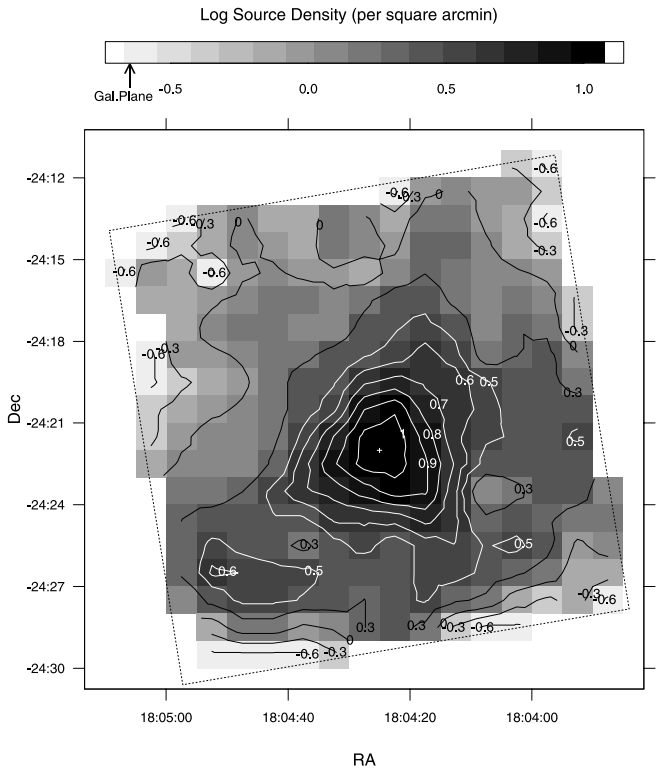

FIG. 6.—Gray-scale map of detected source density in NGC 6530 (only sources with ACIS count rate $\geq 3 \times 10^{-4}$ counts s^{-1}, detectable across the whole ACIS field), with contour levels. The assumed cluster center is indicated by a small cross. The arrow in the top gray scale indicates the average source density in the reference Galactic plane field.

One would like to know just how much of the NGC 6530 cluster falls outside our ACIS FOV. Clues to this may be found in the *ROSAT* PSPC image, which shows that apart a few discrete sources (mainly Herschel 36 to the west and HD 165052 to the east), nearly all of the PSPC unresolved emission falls inside our ACIS field. A similar conclusion may be reached from the *XMM* data (Rauw et al. 2002), covering a larger field than ACIS but pointed about $10'$ to the west of our field. It shows very few sources outside our ACIS FOV toward the west, south, and north, with the exception of Herschel 36 and its immediate neighborhood. We conclude that indeed a very large fraction of the total NGC 6530 cluster is covered by our ACIS FOV.

We have also examined why previous optical studies failed to identify this substantial NGC 6530 cluster population found in our X-ray study. Figure 7 shows spatial distributions of our X-ray sources in two different X-ray luminosity ranges, together with distributions of optical stars brighter and fainter than $V = 15$. The X-ray sources show evident clustering, while optical stars, in either magnitude range, do not (apart from the few bright OB stars, which typically do cluster). For a cluster at the distance of NGC 6530 on the Galactic plane and close to the Galactic center direction, the number of field stars is very large (even though almost no background stars are found in the SCB optical sample, as discussed in § 4.2) and precludes a statistical determination of the cluster population of late spectral types, as noted by previous studies such as The (1960).

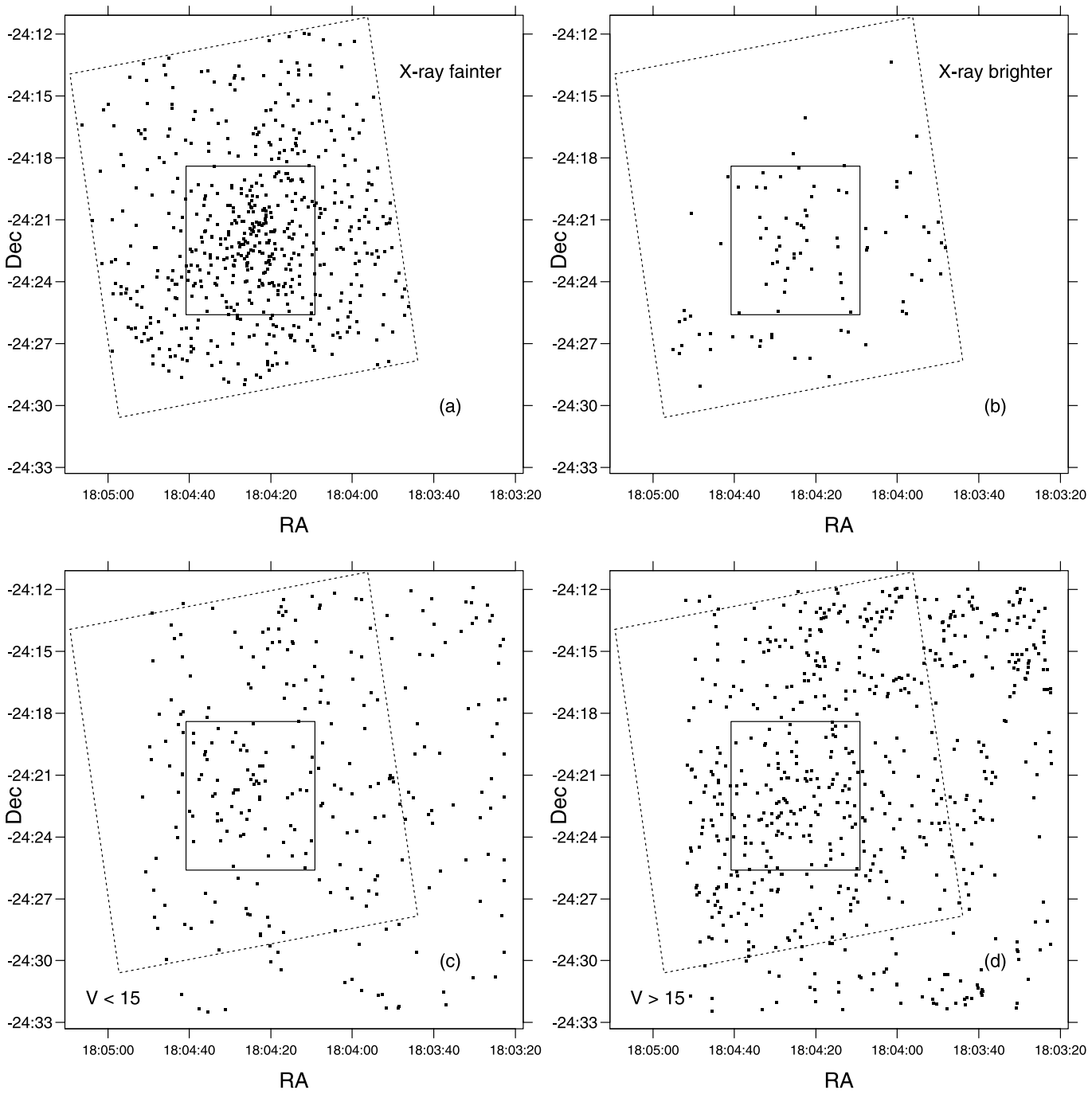

FIG. 7.—Spatial distributions of (*a*) X-ray sources with ACIS count rate in the range 3×10^{-4} to 3×10^{-3} counts s^{-1}, (*b*) X-ray sources with ACIS count rate $\geq3\times10^{-3}$ counts s^{-1}, (*c*) all stars with $V < 15$, and (*d*) all stars with $V \geq 15$. Note that apart from the visually bright stars evident in Fig. 1, there is no obvious clustering of optical stars in any magnitude range, as found in previous studies. The dotted lines indicate the ACIS FOV, while the solid lines indicate a reference square region of 7.′2 on a side, centered on cluster center as defined in Fig. 6.

We have computed the expected number of foreground field stars brighter than $V = 17$ falling in the ACIS FOV toward NGC 6530, which, using data from Allen (1973) for a cluster distance of 1800 pc and average extinction $A_V \sim 1$, turns out to be 720 stars, even larger than the number of X-ray undetected SCB stars in the FOV (391 stars; see § 3.3). For a smaller cluster distance of 1300 pc (Walker 1957), the expected number becomes 356 stars, very close to the observed number. In any case, we do not expect many background stars to be contained in the SCB sample.

Compared to SCB field stars, an even larger density of field stars (both foreground and background) is found in the 2MASS data, as already seen in § 4.2. This emphasizes how crucial sensitive, high-resolution X-ray data are for a proper study of such very young star clusters.

4.4. *H-R Diagram*

To understand better the nature of the stellar population selected through our X-ray data, we have located their optical counterparts on a (V, $V-I$) H-R diagram of the NGC 6530 region using SCB optical data, as shown in Figure 8. A few stars fainter than $V = 17$ are PMS cluster members selected by SCB from their Hα excess.

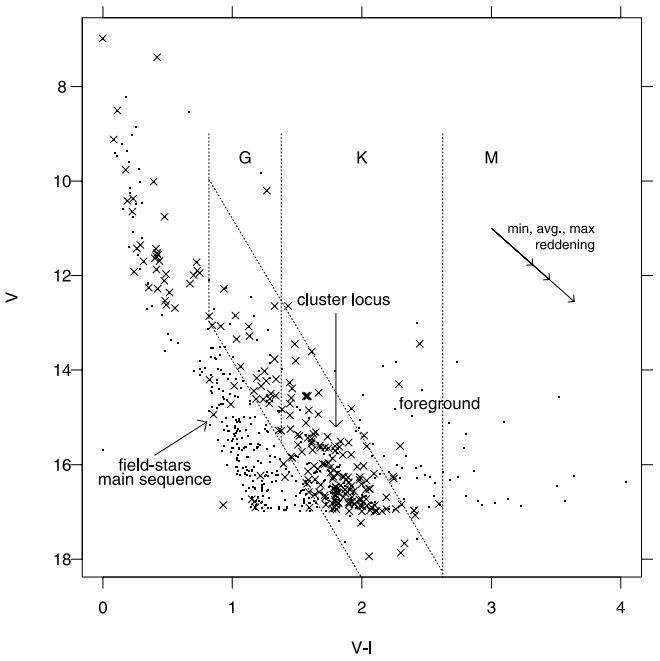

FIG. 8.—Color-magnitude (V, $V-I$) diagram for NGC 6530 (from SCB data). The average reddening correction and its range are indicated. *Crosses*: X-ray–detected stars. *Dots*: X-ray nondetections. A region is indicated where most X-ray–detected stars with G-K (dereddened) $V-I$ color are found, which we call the "cluster locus." Blueward of it, we identify a field-star "main sequence" (an envelope of field-star main sequences up to the cluster distance). Note that there is an apparent lack of stars more distant than NGC 6530, probably because they are completely obscured by the dark cloud just behind the visible cluster. See text.

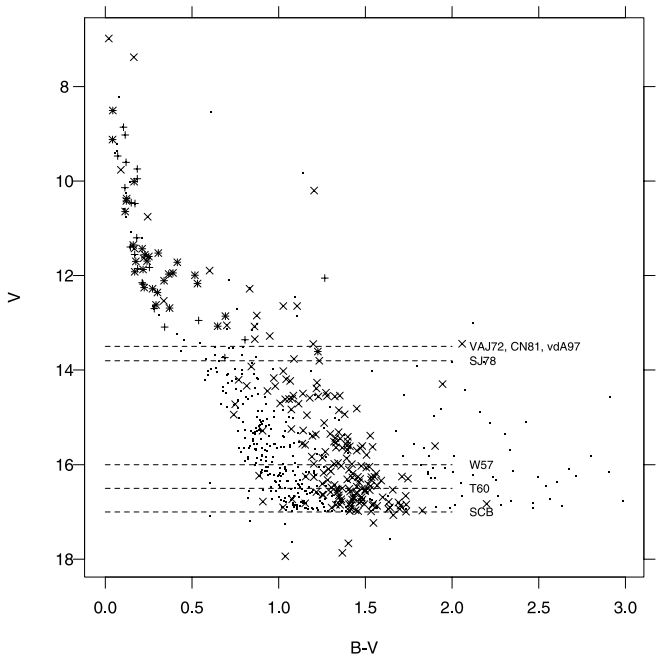

FIG. 9.—Color-magnitude (V, $B-V$) diagram for NGC 6530. *Crosses*: X-ray–detected stars. *Dots*: X-ray nondetections. *Plus signs*: Stars with proper-motion membership probability greater than 50% according to van Altena & Jones (1972) (X-ray–detected, proper-motion members show up as asterisks). Dashed horizontal lines indicate magnitude limits from different optical studies of NGC 6530: van Altena & Jones (1972, VAJ72), Chini & Neckel (1981, CN81), van den Ancker et al. (1997, vdA97), Sagar & Joshi (1978, SJ78), Walker (1957, W57), The (1960, T60), and SCB.

This diagram proves to be very rich in information. Examining Figure 8, we note (1) an upper main sequence (as reddened by SCB and indicated with the vector on the upper right); (2) a swarm of stars whose lower envelope shapes the main sequence at the NGC 6530 distance, mostly undetected in X-rays, labeled "field-star main sequence" in the figure; (3) another swarm of X-ray–detected stars, distinctly to the right of main-sequence field stars and mostly at faint V magnitudes; and (4) with still redder $V-I$ color, a much less numerous population of stars, presumably foreground.

Since we have already established that most stars detected in X-rays are cluster members, the position occupied by the bulk of X-ray detections defines the NGC 6530 cluster locus in the H-R diagram. Accordingly, we have drawn a trapezoidal region enclosing them in Figure 8, with (reddened) colors corresponding to G-K-M stars, and we have labeled it "cluster locus." The number of X-ray–detected G-K stars in the main-sequence and foreground regions is about 12–15, compatible with the estimated number of contaminating field objects among optically identified sources. Therefore, we regard all X-ray detections in the cluster locus as genuine NGC 6530 members, with no more than a few spurious objects among them. On the other hand, the probability that X-ray–detected stars outside the cluster locus belong to the cluster is expected to be very small. In most X-ray studies of star-forming regions with a well-defined member list, e.g., as in the Orion Nebula, X-ray–detected and undetected stars are found to be well mixed in the H-R diagram (see, e.g., Feigelson et al. 2002; Flaccomio et al. 2003a). We therefore assume that there will be hardly any NGC 6530 members among the X-ray–undetected stars that fall outside our cluster locus.

For field stars at distances just a little closer than NGC 6530, the main sequence is very well defined (see § 1) as the lower envelope of dots in Figure 8, with only two stars below it, confirming the absence of background field objects, with the two exceptions probably seen through small holes in the molecular cloud (or perhaps representing foreground white dwarfs). The reddening of background stars must therefore be so large that they would appear at much fainter magnitudes than the SCB catalog limit. The direction of the reddening vector direction, as shown in the figure, is such that stars in the cluster region cannot be more distant, highly reddened stars.

Most X-ray detected stars have the $V-I$ colors of K stars. None have M star colors, probably since M stars in the cluster are fainter than the SCB magnitude limit and all M stars in SCB are low-mass foreground stars. Among stars bluer than G type, we consider all O and B stars in the FOV to be cluster members because of their rarity in the field, as found in previous studies. Stars of intermediate type (A and F) are seen in the H-R diagram of Figure 8 to be mostly X-ray detected if they are brighter than $V = 13$; because of their large number these X-ray sources must also be cluster members. Therefore, we consider all stars earlier than type G and with $V < 13$ to be highly probable cluster members. The percentage of X-ray–detected stars in the range B3–F5 is 49% (25/51) for $V < 13$; including fainter (mostly field) F stars halves this percentage.

In order to compare our NGC 6530 member selection with that of previous optical studies, we show in Figure 9 a (V, $B-V$) diagram for NGC 6530, plotting X-ray–detected and undetected stars, together with stars found by van Altena & Jones (1972) to have a proper-motion membership probability greater than 50%. In addition, we indicate with horizontal lines approximate magnitude limits for various previous

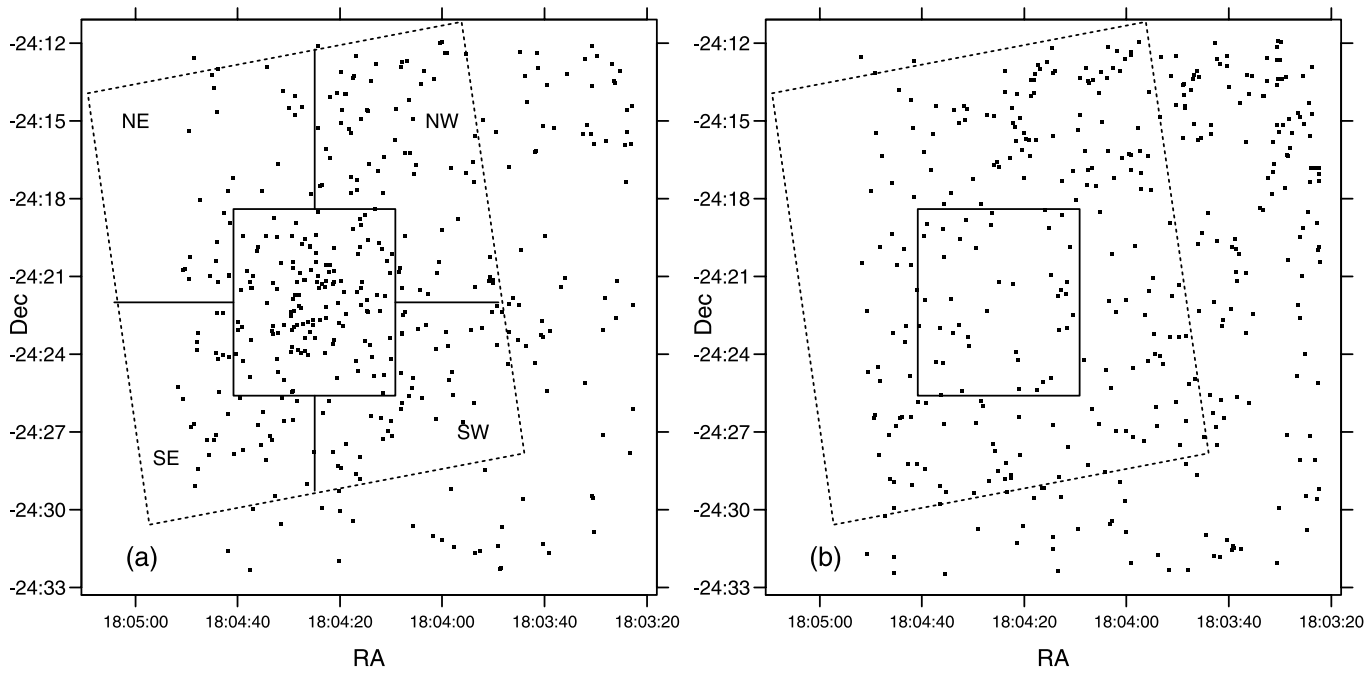

FIG. 10.—Spatial distribution of (*a*) cluster-locus stars and (*b*) main-sequence (putative field) stars, including also stars outside the ACIS field of view. The difference between these distributions is obvious and strengthens our assumptions on the nature of the two subsamples. Also identified in (*a*) are different subregions discussed in the text.

studies (see § 1). A number of early-type stars have low proper-motion membership probability, suggesting that this indicator has limited value. Nevertheless, we find that many stars of types B and A and $V \leq 13$ are both proper-motion members and X-ray detected, strengthening our assertion that these stars are indeed cluster members. The usefulness of the proper-motion study of van Altena & Jones (1972) is confined to these brighter stars because of the study's magnitude limit at around $V = 13.6$. The inability of The (1960) and SCB to detect the lower mass cluster locus can be understood in view of both the large number of field stars and the fact that in such a young cluster low-mass stars are still in their PMS stages. They are regularly found in a wide band above the main sequence in the H-R diagram, not in a narrow and well-defined ZAMS locus. This "dilutes" their appearance on the H-R diagram and makes them unrecognizable against the large number of foreground field stars.

To test the validity of our "cluster locus" selection in the (V, $V-I$) diagram, we plot in Figure 10 the spatial distributions of stars in this locus (Fig. 10*a*) and stars in the main-sequence locus (Fig. 10*b*). It is obvious that while cluster-locus stars are indeed clustered around the NGC 6530 center and are much less numerous outside our ACIS FOV, to the south and to the west, main-sequence field stars are much more evenly distributed across the whole region, with absolutely no clustering toward cluster center. This strengthens our contention that most stars in the cluster locus are indeed cluster members. This locus contains 158 X-ray–detected and 88 X-ray–undetected stars. While the cluster membership is virtually assured for all detections, membership for nondetections is much more uncertain. If the NGC 6530 cluster ends exactly at the edge of our FOV (a reasonable approximation, as discussed above), we can estimate the number of nonmembers in the cluster locus inside our FOV from the space density of cluster-locus objects outside the FOV. A density of 0.41 ± 0.05 cluster-locus stars per square arcminute times the ACIS FOV area common to SCB yields 104 ± 12 field stars in the cluster locus within our ACIS FOV. This number (within uncertainties) is the same as the number of undetected stars in the cluster locus, indicating that most are nonmembers. Since we do not know exactly where the NGC 6530 cluster border lies in the sky, however, this is an overestimate of contamination in the cluster locus, and we will admit in the following also the possibility that a fraction of the X-ray–undetected stars in this locus may be NGC 6530 members.

In the following we therefore regard as confirmed cluster members (1) all O and B stars; (2) all A and F stars brighter than $V = 13$; (3) all X-ray–detected stars falling in the cluster locus of Figure 8; and (4) all Hα-emission PMS stars selected by SCB (including PMS candidates), 39 of which fall in our ACIS FOV, regardless of their X-ray detection. These stars will be collectively indicated as "cluster stars." X-ray–undetected stars falling in the H-R diagram cluster locus are of uncertain status and will be indicated as "possible members."

4.5. *Masses and Ages*

Figure 11 provides a comparison of the H-R diagram positions of stars in our ACIS FOV with the predictions of theoretical PMS evolutionary tracks[3] (Siess et al. 2000, hereafter SDF), reddened using the average NGC 6530 values found by SCB. Here we have omitted all optically bright stars, already on the main sequence, and very red ($V-I > 3$) foreground field stars. Using the SDF models, we have derived from the diagram shown in Figure 11 masses and ages for our cluster stars not yet on the main sequence. The plotted ZAMS in Figure 11 is reddened with the average cluster extinction,

[3] These models have proven to be consistent with dynamical stellar masses (Simon et al. 2000) and have already been used in the interpretation of *Chandra* X-ray data on the Orion Nebula cluster by Flaccomio et al. (2003a, 2003b).

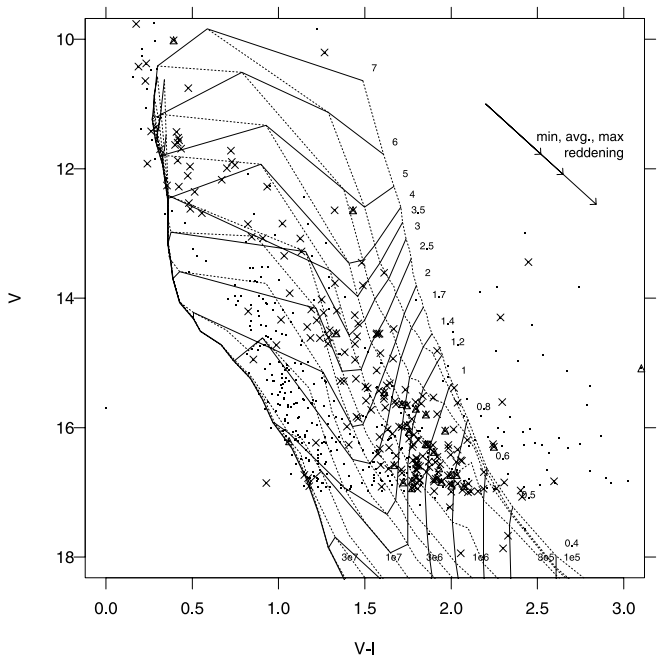

FIG. 11.—Color-magnitude (V, $V-I$) diagram of all stars in the ACIS FOV with $V > 10$, with (reddened) evolutionary tracks (*solid lines*) and isochrones (*dotted lines*) from SDF overlaid. Symbols are as in Fig. 8, with the addition of triangles to indicate optical variable stars. Note that the plotted ZAMS is reddened with the average cluster extinction, while a differently reddened ZAMS is appropriate to field stars.

while a differently reddened ZAMS is appropriate for field stars.

In the figure we have also indicated with triangles optical irregularly variable stars in our ACIS FOV (29 stars) from the General Catalogue of Variable Stars (Kholopov et al. 1998). These stars are typically found in star formation regions among low-mass PMS stars (e.g., T Tauri stars). They share the same locus in the H-R diagram as the X-ray–detected cluster population and are thus stars in the same mass range and evolutionary stages. Ten of these variable stars are also strong Hα emitters, and all but four are detected in X-rays. Only two of these latter four are plausible cluster members from their position in the H-R diagram, one also selected from Hα. Hence including variable stars adds little to the NGC 6530 population already selected.

In Figure 8 we have shown the average reddening found by SCB in NGC 6530, as well as its minimum and maximum value. These values were derived from the ($U-B$, $B-V$) color-color diagram of OB stars. In Paper II we present indications on the basis of our ACIS X-ray spectra that the average absorption of lower mass stars may be higher, on average by a factor of 2 (provided that the thermal structure of these stars' coronae is satisfactorily reproduced by our models and that a constant gas-to-dust ratio is present toward all cluster stars). An examination of the ($U-B$, $B-V$) diagram for all cluster stars (i.e., confirmed members) shows that lower mass stars have a larger scatter than massive stars, indicating a larger range of differential extinction, with higher average values. From Figure 11 we see that differential reddening may displace stars in the H-R diagram along a direction almost parallel to isochrones in the part of the diagram where most cluster stars are found. Therefore, age estimates are little affected by extinction uncertainties (within twice the range found by SCB), while mass estimates are much more affected (for example, a star with $M = 1\ M_{\odot}$ may be mistaken for a more reddened star with $M = 1.5\ M_{\odot}$). Masses for possibly embedded objects are instead much more uncertain.

Figure 12*a* shows the age distributions of NGC 6530 members found in different nonoverlapping subregions, namely a central region plus four outer regions. Despite a large scatter,

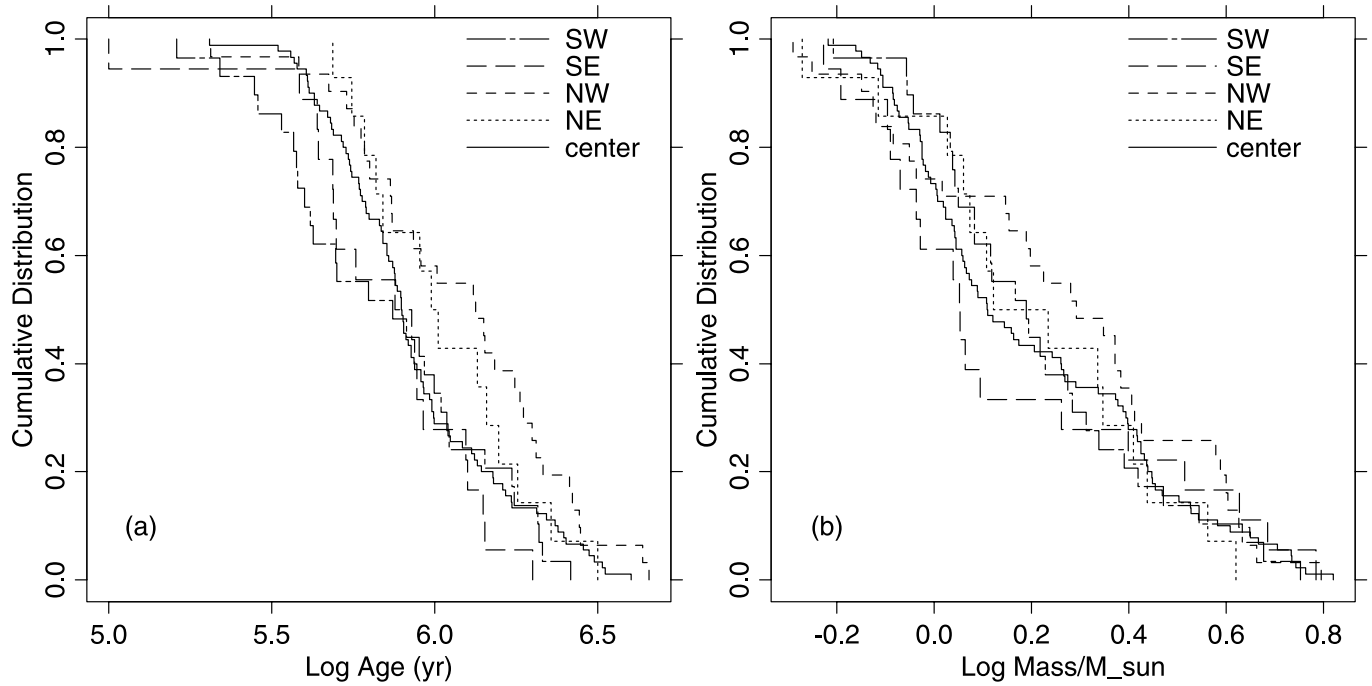

FIG. 12.—Age and mass distributions for X-ray–detected stars in the cluster locus belonging to different spatial regions, identified in Fig. 10. (*a*) Age distribution. There is a clear age difference between the selected samples in different regions, especially between the northwest and southeast regions. (*b*) Mass distribution. A difference is visible, but this may be due to the combined effect of an age difference and the optical photometry V limit.

there is a systematic difference between these regions: stars in the northwestern outer region appear to be definitely older than stars in the cluster center. To a lesser extent this is true also of stars in the northeast. On the contrary, stars in the southeast are on average younger than cluster center, with a smaller spread, while stars in the southwest seem to have a mixture of ages, some similar to cluster center and some much younger. This southwest subregion apparently contains a heterogeneous stellar population with an age spread larger than elsewhere in the cluster. It is also closest to the Hourglass region, which contains the very young star Herschel 36.

On the basis of the "displacement" between the NGC 6530 stellar cluster and the more embedded, probably protostellar object Herschel 36 and the Hourglass Nebula, it has been proposed that star formation in this region occurred in a sequence starting near the NGC 6530 center and proceeding toward west. In this scenario, one would expect to find younger stars in the western part of our FOV, lying very close to the Hourglass. Our data suggest instead a different scenario, where star formation has progressed from north to south, not from east to west. Stars in the northwest were the initial generation of stars, now fully emerged out of the molecular cloud (stars in this region are found in Paper II to have the smallest X-ray absorption). Then the bulk of the cluster formed (in the central region), and later stars formed more to the south and southwest (including the Hourglass region). This can be seen more clearly from Figure 13, which plots the spatial distributions of cluster stars in three different age ranges: age less than 5×10^5 yr (*filled circles*), age between 5×10^5 and 2×10^6 yr (*plus signs*), and age greater than 2×10^6 yr (*open circles*). It is obvious that very young stars are dominant in the south/southwest, comprise a smaller fraction in the center, and are totally absent in the northwest.

It is also interesting to note that the very young stars found in the south share the same spatial distribution as the X-ray flaring sources (see § 4.7). Moreover, the X-ray–bright stars in the southeast follow rather closely the shape of an Hα bright rim, which is evident at the bottom left of Figure 1 and appears to be the edge of a denser portion of the molecular cloud, excited by the radiation of the nearby O stars (primarily 9 Sgr) and probably also compressed by the winds of the massive star(s). In the same region, Tothill et al. (2002) have found a series of molecular cloud cores, probably undergoing collapse. The association of a very young PMS group and a perturbed, compressed cloud is not likely to be accidental; it is probably instead an example of genuine induced star formation, caused by the action of nearby massive stars.

The median age of cluster stars in the central region is 8×10^5 yr, slightly younger than the 1.5 Myr derived by SCB for the massive NGC 6530 stars and compatible with the possible ages that they find for low-mass PMS stars. Since there may be uncertainties in the evolutionary models, especially when comparing high- and low-mass stars, we regard high- and low-mass stars in the same NGC 6530 subregion as essentially coeval. This age similarity between massive and low-mass stars is unlike that found in another very young cluster, NGC 6231, where Sung et al. (1998) find that the low-mass stars are much older than massive stars. The age spread that we observe for the whole NGC 6530 cluster is similar to that (4 Myr) found by SCB, while the age spread that we find in each subregion is smaller.

Because X-rays with energies above 1 keV can emerge from deep within a molecular cloud, our sample probably contains

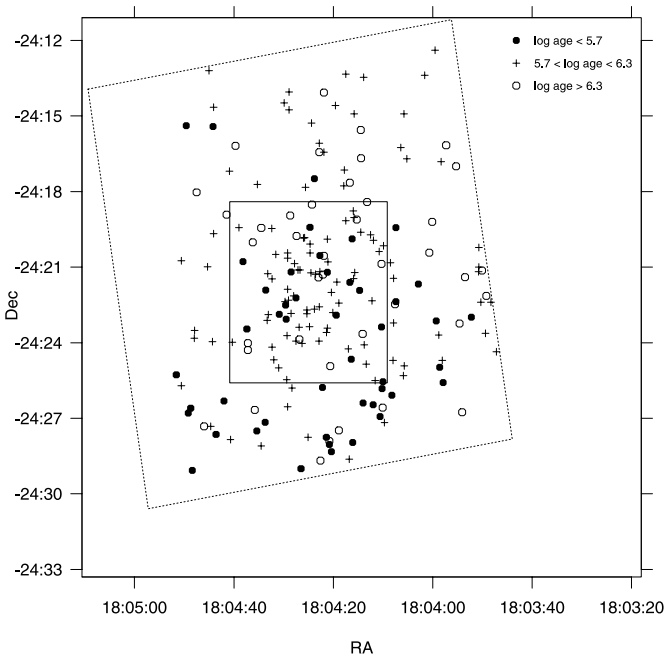

FIG. 13.—Spatial distribution of X-ray–detected stars in three different age ranges. *Filled circles*: log age < 5.7 Myr. *Plus signs*: log age between 5.7 and 6.3 Myr. *Open circles*: log age > 6.3 Myr. Note the prevalence of very young stars in the southern part.

stars much more reddened than found by SCB. However, a difference in reddening between stars in the northwest and those in the south is unlikely to be the only reason why these stars appear to have different ages. Since age is relatively insensitive to reddening in this part of the H-R diagram, a large reddening for the southern stars should be invoked to make all stars have the same age. If this were the case, stars in the south would be fainter and harder to detect, both in the optical and X-rays. But in this region there is no deficit of optical stellar counterparts; instead there is an excess of (bright) X-ray sources with respect to northern regions. Moreover, a difference only in reddening would not explain the spatial coincidence of these apparently younger stars with flaring X-ray sources. Nor are the flaring sources more absorbed than other X-ray sources: as noted in §§ 4.7 and 4.8, flaring sources and strongly absorbed X-ray sources have very different spatial distributions, with the latter uniformly spread over the FOV, not concentrated toward the south.

We have also studied the distribution of stellar masses in the same subregions, as shown in Figure 12*b*. An apparent correspondence between the age and mass distributions, i.e., with older (younger) regions containing also more (less) massive stars and vice versa, is very likely due to a selection effect of the combination of the evolutionary path of low-mass stars in the H-R diagram with the V magnitude limit of the SCB catalog. If the stars in a region are younger, they are still high on their Hayashi tracks, and therefore stars of lower masses are above our magnitude limit. On the other hand, in an older region only more massive stars are above the same limit. Therefore, with the current magnitude limit it is difficult to discriminate between an age and a mass effect (but at least one of the two is really present). Moreover, mass determinations from evolutionary tracks are more sensitive to reddening uncertainties than age determinations. The magnitude limit of the SCB catalog ensures that we have a complete sample of stars with masses

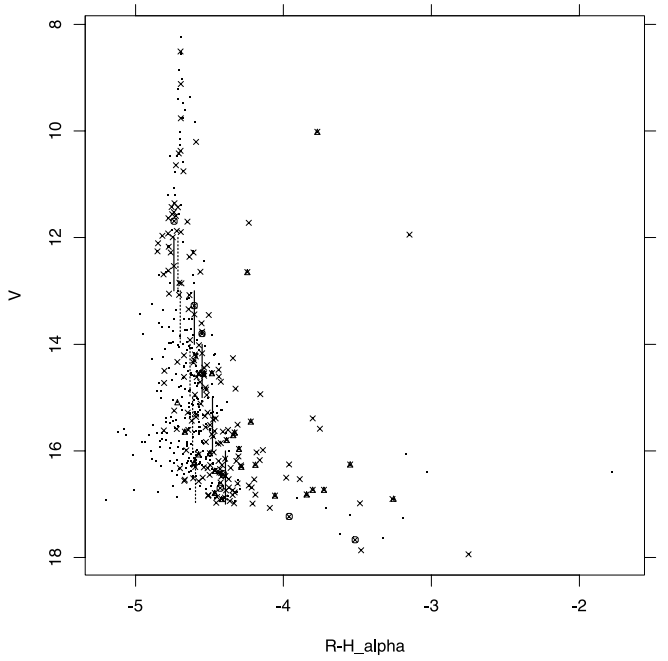

FIG. 14.—Diagram (V, $R-\mathrm{H}\alpha$) for the whole NGC 6530 ACIS field. *Crosses*: X-ray–detected stars. *Dots*: X-ray nondetections. *Open circles*: Stars exhibiting X-ray flares. *Triangles*: Optically variable stars. Stars with Hα excess appear on the right part of this diagram, and not all are X-ray detected. Solid and dotted vertical segments indicate median $R-\mathrm{H}\alpha$ values for X-ray–detected and undetected stars, respectively, in different V magnitude intervals.

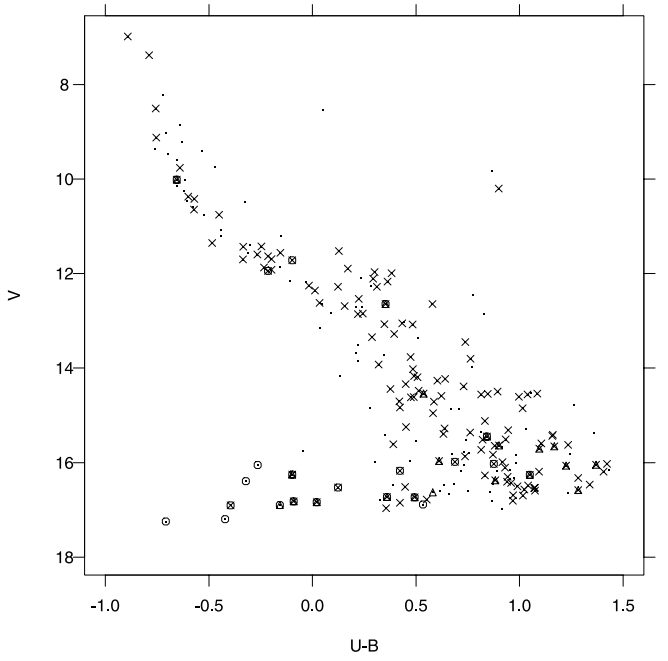

FIG. 15.—Color-magnitude (V, $U-B$) diagram for NGC 6530. For $V > 13$, only stars in the cluster locus are plotted. *Crosses*: X-ray–detected stars. *Dots*: X-ray nondetections. *Circles*: Hα-excess stars. *Triangles*: Optical variable stars. Stars with $V > 16$ and $U-B < 0.25$ have strong violet excesses.

above 1.5 $M_\odot$, while the coverage of lower mass stars is increasingly less complete, with the lowest selected cluster members having a mass of 0.5 $M_\odot$ (Fig. 11).

A mass segregation effect with the (apparent) observed pattern, however, namely a south-to-north mass gradient whereas the bulk of the cluster lies in the middle, seems highly unlikely, and we therefore strongly favor the age-evolution interpretation rather than a mass-difference one. To settle this question definitively, a deeper photometric catalog is needed, and one will be available in the near future (Prisinzano et al. 2004).

4.6. *Stars with* Hα *Emission*

We have compared the cluster population selected in X-rays with that selected using Hα by SCB in Figure 14, a (V, $R-\mathrm{H}\alpha$) diagram, where $R-\mathrm{H}\alpha$ is the Hα emission index reported by SCB. Stars with strong Hα emission are found in the right part of this diagram. Triangles indicate optical variables, some of which are also stars with strong Hα, while open circles represent stars exhibiting X-ray flares, two of which are also strong Hα stars.

First, we note that 10 stars with strong Hα are not detected in X-rays, a sizable fraction of the total number of strong Hα stars. These stars are confirmed cluster members both because of their Hα emission and because of their position in the H-R diagram. On the other hand, most X-ray–detected stars (confirmed members as well) have an Hα emission not distinctly different from X-ray–undetected stars (mostly nonmembers). Therefore, X-ray and Hα observations provide two complementary means of selecting low-mass PMS stars in a star-forming region such as NGC 6530, with stars escaping one method being easily found by the other. It should be pointed out, however, that within the magnitude limit of the SCB catalog, X-ray imaging appears to be much more efficient in selecting these PMS stars.

In the figure, solid and dotted segments indicate median $R-\mathrm{H}\alpha$ values for X-ray–detected and undetected stars, respectively, in different V magnitude intervals. Although no clear-cut separation is present, X-ray–detected stars have systematically larger $R-\mathrm{H}\alpha$ indices than undetected stars. The median $R-\mathrm{H}\alpha$ values (not shown) for X-ray–undetected cluster-locus stars are close to the rest of the undetected stars in all magnitude ranges, suggesting again that most of these stars are not cluster members, as already found in § 4.4. The behavior found for X-ray–detected stars indicates that most cluster stars, although not showing a very strong Hα emission, have some Hα emission in excess of the main-sequence star level. This might be due to enhanced chromospheric activity, which parallels enhanced X-ray activity in stars of very young ages, or to residual circumstellar phenomena, where the star interacts with a surrounding accretion disk, as is thought to happen in strong-Hα stars. This latter option is possibly favored, since at the very young age found for NGC 6530 stars most stars in other star-forming regions (e.g., Orion) are found to have still an accretion disk and to interact with it to some extent. While a more precise classification of these stars must wait for high-resolution optical spectra of these stars, some clues may come from the analysis of the just released IR data from the 2MASS survey. This is however beyond the scope of this paper. A detailed analysis of the respective X-ray emission levels of weak- and strong-Hα stars, and of the connection between PMS accretion and X-rays, will be presented in Paper II.

Since another indicator of circumstellar accretion in PMS stars is UV excess, we have also studied where our cluster-locus stars fall in a (V, $U-B$) diagram, shown in Figure 15 (field stars are not plotted). In this plot, we have also indicated Hα-emission stars with circles. At least a dozen stars in the cluster locus have strong violet excesses, suggesting active

PMS accretion. Most of them have $V \geq 16$ and $V-I$ colors of K stars. Nearly all of the UV excess stars are already selected as members either through Hα (most of them) or X-rays (a smaller number), and therefore a UV selection would not add much to our knowledge of the cluster. Eight UV-excess stars are also optical variables.

4.7. *X-Ray Variables*

Some of our X-ray sources show flare-like X-ray variability (see § 4.6). While this will be studied in detail in a further paper (F. Damiani et al. 2004, in preparation, hereafter Paper III), we discuss here some implications for the study of the cluster population. Various types of X-ray variability are found in NGC 6530, but here we focus only on sources showing "classical" X-ray flares.

Figure 16 shows the spatial distribution of flaring X-ray sources (*filled circles*). The spatial nonuniformity is obvious and with good source statistics. This distribution, heavily concentrated toward the south-southwest, is very similar to the distributions both of the youngest cluster stars (Fig. 13) and of the brightest X-ray sources (Fig. 7*b*), while it is unlike the distribution of the bulk of X-ray–detected sources (Fig. 7*a*). We therefore conclude that in NGC 6530 frequent and intense X-ray flares are preferentially associated with the youngest of PMS stars and decline rapidly afterward, even at ages of only 2 Myr (typically found in the northwest region, where only few flaring stars are found).

By comparison, stars with strong Hα emission in NGC 6530 are characterized by a much broader spatial distribution, across practically the entire cluster (Fig. 16, *circles*). In other star formation regions, Hα emission is found in PMS stars with a large range of ages and thus not only in the earliest phases of evolution. In the H-R diagram, it is often found that strong-Hα stars share their locus with weak-Hα stars, so the timescales for decrease of circumstellar activity vary from star to star, over a wide range. This indicates that strong X-ray flaring is a more typical feature of the very youngest PMS stars than strong Hα emission is.

4.8. *Hard X-Ray Sources*

We now study the subset of detected X-ray sources with hard X-ray spectra, defined as having at least three-quarters of the total counts with energy above 1.5 keV. At these X-ray energies, absorption is much smaller compared to lower energies, providing an opportunity to peer deeper into the cloud or even to detect background objects unrelated to the cluster.

In our ACIS FOV we find 101 such hard sources, of which only seven have an optical counterpart in the SCB catalog, a much smaller fraction than the overall fraction of optically identified X-ray sources (24.9%). The counterparts of most hard sources are therefore either very faint and/or heavily obscured objects. The number of hard sources is compatible with the hypothesis that all of them are background objects (see § 4.1). However, the ACIS count-rate distribution of such sources has a median of 4.3×10^{-4} counts s^{-1}, intermediate between the median count rate of the whole NGC 6530 field (5.9×10^{-4} counts s^{-1}) and that of the reference Galactic plane field of § 4.1 (2.9×10^{-4} counts s^{-1}). In the Galactic plane field, absorption of distant objects is not as large as in our NGC 6530 field. If it were the same, the hard sources would be detected with higher count rates, becoming thus even less compatible with the Galactic plane values. Therefore, this hard-source subsample is unlikely to be composed predominantly of background objects, but rather should be largely composed of embedded cluster members.

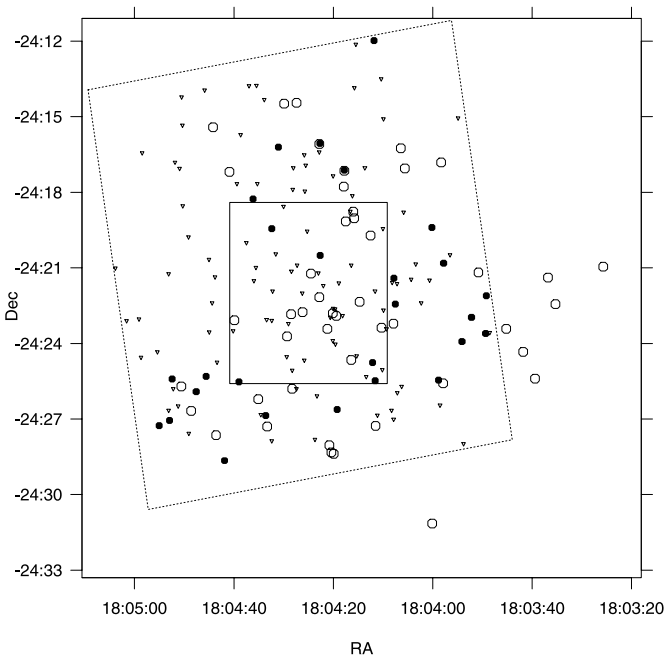

FIG. 16.—*Filled circles*: Spatial distribution of X-ray sources showing flares, which is different from the spatial distribution of the bulk of X-ray–detected sources (Fig. 7*a*) but very similar to that of the very young cluster stars shown in Fig. 13. *Open circles*: Hα-excess stars, which have a more uniform distribution across the cluster. *Small triangles*: Hard X-ray sources. Their space distribution is more uniform compared with the cluster locus distribution of Fig. 10*a*.

To verify this, we have plotted in Figure 16 the spatial distribution of such hard X-ray sources (*small triangles*). They are spread across the FOV much more uniformly than either optical stars in the cluster locus (Fig. 10*a*) or the bulk of X-ray sources (Fig. 7*a*), with at most a moderate clustering toward the center (partly caused by the lower on-axis detection threshold). This hard-source population appears to be different from (most of) the cluster population; since a subset of these hard sources probably belongs to the cluster, this "cloud embedded" population appears to be less concentrated than the exposed part of the cluster and may constitute another step in the star formation sequence in this region.

Four hard X-ray sources have enough counts for a spectral analysis (see Paper II), and in all cases the best-fit absorption is found to be $\log N_{\rm H} = 22.7-22.8$ (cm^{-2}), more than 10 times the absorption of most cluster X-ray sources.

Our X-ray data alone are insufficient to study this embedded population in greater detail. Deep IR images, which will also permit the study of objects in the interior of the cloud or beyond it, would probably contribute significantly to this. A comparison of this hard-source population with the recently released 2MASS IR data will be given in Paper II.

Only two objects (in the southeast, neither optically identified) are common to both the hard-source and the X-ray flaring samples, indicating that these hard X-ray sources are no more eruptive than cluster stars.

5. DISCUSSION

With a single deep, high-resolution *Chandra* X-ray observation of NGC 6530, we have gained a large amount of information on the stellar population of the cluster. Perhaps the

single most important result is that NGC 6530 contains a population of at least 800 low-mass PMS stars; a deeper X-ray study would probably find more. Most of these low-mass stars have escaped all previous studies: only a few tens were previously known as either Hα emitters or variable stars. Our X-ray observation is so deep that about three-quarters of the detected X-ray sources have counterparts fainter than the $V = 17$ limit of the deepest available catalog of NGC 6530 optical stars by SCB. Even within this magnitude limit, our X-ray data have permitted the selection of about 180 PMS cluster members, compared with the 46 PMS members from the Hα study of SCB. *Chandra* X-ray observations have therefore proven to be by far the most efficient way to select low-mass PMS stars in a massive and distant (1800 pc) cluster such as NGC 6530. There is some complementarity between X-ray and Hα selection, since the strongest Hα emitters are not detected in X-rays, but the largest PMS samples cannot be selected in an Hα survey such as that of SCB.

As a consequence, the NGC 6530 initial mass function (IMF) in the low-mass range, previously derived mostly from Hα studies (SCB), must be taken with caution. There are far more low-mass stars than found by SCB, and while they estimated that the Hα selection completeness was about 50%, our new data show it is only half that value (at most) down to $V = 17$. Moreover, this value likely depends on the particular star-forming region and on the optical survey limit, since a value close to 50% was found in NGC 2264 by Flaccomio et al. (2000). Therefore, an extrapolation of results from Hα studies is unreliable, while a much more complete study is possible using X-ray selection of members. For NGC 6530 X-ray–selected PMS stars, we have a rather limited and age-dependent mass completeness (see § 4.5) because of the optical catalog used, and therefore we have not attempted to derive the cluster IMF in this work. This will be done in a forthcoming paper on the basis of deeper optical photometry (Prisinzano et al. 2004).

In addition to deeper optical photometry, many data are still missing for a more complete knowledge of the stellar census of NGC 6530: deep Hα surveys, which have the potential of discovering X-ray–undetected cluster stars, and lithium abundance and radial velocity surveys, capable of selecting members independently of their X-ray or Hα emission. To date, only the brighter cluster members have a spectroscopically determined spectral type. Also, a deeper study of the existing 2MASS data on NGC 6530 will probably yield important insights on the cluster population and its evolution.

Another important result of the present study is the apparent presence of an age gradient across NGC 6530, with an older and more exposed region in the northwest contrasting with a younger, more embedded region in the south and southwest. This supports the idea of sequential formation, already proposed for the NGC 6530 region by Lada et al. (1976), although with a different pattern. In such a sequence, the bulk of NGC 6530 stars (including most bright stars) is found at intermediate ages in the central cluster region, suggesting that star formation proceeds slowly at the beginning and then reaches a maximum rate and declines afterward, spreading to outer cloud regions, possibly triggered by the momentum injected in the cloud medium by the massive stars just formed in the cluster. A more detailed study requires deeper photometry to allow the placement on the H-R diagram of a larger number of X-ray–selected cluster members.

This picture resembles qualitatively that proposed recently by Palla & Stahler (2002) for star formation in the Taurus region, despite differences between these clusters (in density and number of stars) and the different quality of the available data.

It is also interesting to study the (projected) speed at which the disturbance that has caused the sequence of star formation events in NGC 6530 has progressed through the cloud medium. There is probably a formation sequence from cluster center toward southeast and southwest, where the youngest stars are found, but since very young stars are found in the central region as well, it is difficult to assign an age difference between these subgroups. A clearer view is instead obtained by comparing the distinctly different southeast and northwest regions. These two groups of stars, with typical ages of $\sim$0.5 and $\sim$1.5 Myr, respectively, lie about $15'$ apart from one another. At the cluster distance (1800 pc), this distance is equivalent to 7.85 pc. Therefore, the disturbance speed is 7.85 pc Myr^{-1}, or 7.5 km s^{-1}. This is much higher than the sound speed in a cold molecular cloud but is comparable to the sound speed in a hotter H II region (e.g., Spitzer 1978) such as M8, where NGC 6530 is found immersed. A lower speed for the disturbance in the primordial NGC 6530 when neither massive stars nor the H II region had yet formed may explain why star formation proceeded more slowly at the beginning. All things considered, it is hardly surprising to find nonsimultaneous star formation over as large a region as NGC 6530. At the least, one would expect a center-to-border age gradient, as is found in the Orion Nebula (unless an unknown large-scale synchronization mechanism were operating).

It is also interesting to note the similarity of this disturbance speed just derived with the results presented by Lada et al. (1976), namely that the M8 H II region is moving toward the observer relative to the background molecular (CO) cloud at a relative speed of 7 km s^{-1}, nearly the same as our value (which however refers to the transverse direction). Moreover, the Lada et al. CO "bright spot 3" is nearly coincident with the NGC 6530 cluster, and across it they observe a radial velocity gradient of ^{12}CO along north-south: the southern emission is blueshifted with respect to cluster center by $\sim$5 km s^{-1}, and they note that it is difficult to interpret this as coherent cloud motion. This, together with our previous findings, suggests that the "disturbance" triggering star formation in NGC 6530 is not like a shock/sound wave in a static medium but is more probably an expansion of one part of the molecular cloud with respect to another, more dense, cold and massive part.

6. SUMMARY

We have made a deep X-ray study of the very young cluster NGC 6530 using the *Chandra* ACIS. Our main results include the following:

1. We have detected 884 X-ray point sources strongly clustered around the NGC 6530 center and argue that more than 800 of them are cluster members, a significant increase in the known NGC 6530 population at low and intermediate masses.

2. The optical counterparts of these X-ray sources are found in a band in the H-R diagram lying above the main sequence at the cluster distance and coincident with the predicted locus of 0.5–1.5 Myr PMS stars, mostly of low mass down to 0.5–1.5 $M_{\odot}$.

3. Although three-quarters of the total X-ray detections are yet to be identified optically, we argue that they are probably lower mass cluster members. This is supported also by the 2MASS identification, available for 731 X-ray sources.

4. Finding an age difference between cluster stars in the northwest and those in the south of the observed region, we propose that sequential formation has occurred in NGC 6530.

5. We find that X-ray and Hα selection criteria are complementary, but the completeness of X-ray selection is much larger than that of Hα selection in NGC 6530.

6. We find a number of flaring X-ray sources whose spatial distribution suggests extremely young ages and supports an age difference across the cluster.

7. We find a population of hard X-ray sources, which may be either background objects and/or a more embedded cluster population.

We wish to thank the referee, Marc Gagné, for his stimulating comments and suggestions. This study has made use of data from the SIMBAD database, operated at the Centre de Données Astronomiques, Strasbourg. F. D., E. F., G. M., and S. S. acknowledge support from the Italian ASI and MIUR. S. S. M. and F. R. H. gratefully acknowledge partial support of NASA contract NAS8-38248.

REFERENCES

Allen, C. W. 1973, Astrophysical Quantities (3rd ed.; London: Athlone)
Chini, R., & Neckel, T. 1981, A&A, 102, 171
Cutri, R. M., et al. 2003, Explanatory Supplement to the 2MASS All Sky Data Release (Pasadena: Caltech), http://www.ipac.caltech.edu/2mass/releases/allsky/doc/explsup.html
Damiani, F., Flaccomio, E., Micela, G., Sciortino, S., Harnden, F. R., Murray, S. S., Wolk, S. J., & Jeffries, R. D. 2003, ApJ, 588, 1009
Damiani, F., Maggio, A., Micela, G., & Sciortino, S. 1997a, ApJ, 483, 350
———. 1997b, ApJ, 483, 370
Ebisawa, K., Maeda, Y., Kaneda, H., & Yamauchi, S. 2001, Science, 293, 1633
Feigelson, E. D., Broos, P., Gaffney, J. A., Garmire, G., Hillenbrand, L. A., Pravdo, S. H., Townsley, L., & Tsuboi, Y. 2002, ApJ, 574, 258
Flaccomio, E., Damiani, F., Micela, G., Sciortino, S., Harnden, F. R., Murray, S. S., & Wolk, S. J. 2003a, ApJ, 582, 382
———. 2003b, ApJ, 582, 398
Flaccomio, E., Micela, G., Sciortino, S., Damiani, F., Favata, F., Harnden, F. R., & Schachter, J. 2000, A&A, 355, 651
Harnden, F. R., et al. 2001, ApJ, 547, L141
Hillenbrand, L. A. 1997, AJ, 113, 1733
Kholopov, P. N., et al. 1998, Combined General Catalogue of Variable Stars (4.1 ed.; Moscow: Sternberg Astron. Inst.)
Kilambi, G. C. 1977, MNRAS, 178, 423
Lada, C. J., Gottlieb, C. A., Gottlieb, E. W., & Gull, T. R. 1976, ApJ, 203, 159
Palla, F., & Stahler, S. W. 2002, ApJ, 581, 1194
Prisinzano, L., et al. 2004, A&A, submitted
Rauw, G., Nazé, Y., Gosset, E., Stevens, I. R., Blomme, R., Corcoran, M. F., Pittard, J. M., & Runacres, M. C. 2002, A&A, 395, 499
Rieke, G. H., & Lebofsky, M. J. 1985, ApJ, 288, 618
Sagar, R., & Joshi, U. C. 1978, MNRAS, 184, 467
Siess, L., Dufour, E., & Forestini, M. 2000, A&A, 358, 593 (SDF)
Simon, M., Dutrey, A., & Guilloteau, S. 2000, ApJ, 545, 1034
Spitzer, L. 1978, Physical Processes in the Interstellar Medium (New York: Wiley)
Sung, H., Bessell, M. S., & Lee, S. 1998, AJ, 115, 734
Sung, H., Chun, M., & Bessell, M. S. 2000, AJ, 120, 333 (SCB)
The, P. 1960, ApJ, 132, 40
Tothill, N. F. H., White, G. J., Matthews, H. E., McCutcheon, W. H., McCaughrean, M. J., & Kenworthy, M. A. 2002, ApJ, 580, 285
Townsley, L. K., Broos, P. S., Garmire, G. P., & Nousek, J. A. 2000, ApJ, 534, L139
van Altena, W. F., & Jones, B. F. 1972, A&A, 20, 425
van den Ancker, M. E., The, P. S., Feinstein, A., Vazquez, R. A., de Winter, D., & Perez, M. R. 1997, A&AS, 123, 63
Walker, M. F. 1957, ApJ, 125, 636
Weisskopf, M. C., Brinkman, B., Canizares, C., Garmire, G., Murray, S., & Van Speybroeck, L. P. 2002, PASP, 114, 1